Heavy Water Reactions with Atomic Transition-Metal and Main-Group Cations: Gas Phase Room-Temperature Kinetics and Periodicities in Reactivity

Ping Cheng, Gregory K. Koyanagi, and Diethard K. Bohme*

Department of Chemistry, Centre for Research in Mass Spectrometry and Centre for Research in Earth and Space Science, York University, Toronto, Ontario, Canada, M3J 1P3

Received: April 4, 2007; In Final Form: June 20, 2007

Reactions of heavy water, D_2O, have been measured with 46 atomic metal cations at room temperature in a helium bath gas at 0.35 Torr using an inductively coupled plasma/selected ion flow tube tandem mass spectrometer. The atomic cations were produced at ca. 5500 K in an ICP source and were allowed to decay radiatively and thermalize by collisions with Ar and He atoms prior to reaction. Rate coefficients and product distributions are reported for the reactions of fourth-row atomic cations from K^+ to Se^+, of fifth-row atomic cations from Rb^+ to Te^+ (excluding Tc^+), and of sixth-row atomic cations from Cs^+ to Bi^+. Primary reaction channels were observed leading to O-atom transfer, OD transfer, and D_2O addition. O-Atom transfer occurs almost exclusively (≥90%) in the reactions with most early transition-metal cations (Sc^+, Ti^+, V^+, Y^+, Zr^+, Nb^+, Mo^+, Hf^+, Ta^+, and W^+) and to a minor extent (10%) with one main-group cation (As^+). OD transfer is observed to occur only with three cations (Sr^+, Ba^+, and La^+). Other cations, including most late transition and main-group cations, were observed to react with D_2O exclusively and slowly by D_2O addition or not at all. O-Atom transfer proceeds with rate coefficients in the range of 8.1×10^{-13} (As^+) to 9.5×10^{-10} (Y^+) cm^3 $molecule^{-1}$ s^{-1} and with efficiencies below 0.1 and even below 0.01 for the fourth-row atomic cations V^+ (0.0032) and As^+ (0.0036). These low efficiencies can be understood in terms of the change in spin required to proceed from the reactant to the product potential energy surfaces. Higher order reactions are also measured. The primary products, NbO^+, TaO^+, MoO^+, and WO^+, are observed to react further with D_2O by O-atom transfer, and ZrO^+ and HfO^+ react further through OD group abstraction. Up to five D_2O molecules were observed to add sequentially to selected M^+ and MO^+ as well as MO_2^+ cations and four to MO_2D^+. Equilibrium measurements for sequential D_2O addition to M^+ are also reported. The periodic variation in the efficiency (k/k_c) of the first addition of D_2O appears to be similar to the periodic variation in the standard free energy ($\Delta G°$) of hydration.

1. Introduction

There is much interest in fundamental aspects of the chemistry of atomic cations, especially atomic metal cations. Bare and ligated atomic cations generally play an important role in physics, chemistry, and biology. Water, of course, is practically omnipresent and so is an obvious molecular target for atomic cations found in natural environments such as the earth's ionosphere but also in man-made devices such as mass spectrometers designed to handle atomic cations in which water is often present as a background impurity.

In the mass spectrometer developed in our own laboratory, atomic cations can be generated almost universally in an inductively coupled plasma (ICP) ion source, injected into a flow tube flushed with helium gas at room temperature, and then reacted with water vapor. With the addition of mass selection of the ions entering and emerging from the flow tube, the resulting inductively coupled selected ion flow tube (ICP/SIFT) tandem mass spectrometer allows for surveys of trends in the room-temperature chemical kinetics of reactions with atomic cations across and down the periodic table. For example, reactions of fourth-, fifth-, and sixth-row atomic cations have recently been surveyed with molecular oxygen,[1] both in the absence and in the presence of benzene,[2] and with hexafluorobenzene,[3] N_2O,[4] CO_2,[5] CS_2,[6] and CH_3F.[7] Here, we report the results obtained for reactions of atomic cations with D_2O (D_2O was chosen instead of H_2O to relax the resolution requirements in the downstream mass spectrometer and to distinguish between added and background water).

The first gas phase reactions of atomic metal cations measured with D_2O were those of Na^+ and K^+ reported in 1971 by Biondi's group.[8] The metal cations were produced with a hot filament coated with the oxide of the alkali metal, and rate coefficients for their reactions were measured in a drift tube mass spectrometer over an energy range from thermal energies to 5 eV (mean kinetic energy). This work was followed more than 15 years later by various studies of the interactions of water with other atomic metal cations, especially atomic transition-metal cations.[9−16]

The thermal energy reaction of Ti^+ with H_2O has been investigated with a drift tube and a fast-flow reactor with He as the buffer gas in the pressure range from 0.2 to 0.7 Torr.[12,16] The reactions of fourth-row atomic transition-metal cations of heavy water were studied systematically as a function of translational energy with a guided ion beam tandem mass spectrometer by Armentrout et al.[10] Experimental results were obtained for reactions with Sc^+ and Ti^+,[10] Fe^+,[17] V^+,[18] and Co^+.[19] In these measurements, the atomic cations were produced

* Corresponding author. E-mail: dkbohme@yorku.ca; phone: (416) 736-2100, ext 66188; fax: (416) 736-5936.

10.1021/jp072661p CCC: $37.00
Published on Web 08/16/2007

with a variety of ion sources including surface ionization, electron impact, and flow tube ion sources, in part to try to discern the influence of electronic excitation of the atomic cations on reactivity. The ground-state reactions of Sc^+, Ti^+, and V^+ were shown to be exothermic at thermal energy, whereas the reactions with Fe^+ and Co^+ exhibited endothermic behavior. These authors also investigated the solvation of metal cations by water and reported sequential bond energies for $M^+(D_2O)_n$ with $n = 1-4$ and $M = Na^+$, Mg^+, or Al^{+}[20] and transition-metal cations from Ti^+ to Cu^+.[21] Measurements of the energetics of hydration of alkali ions also were reported by Kebarle et al., who used high-pressure ion source (HPIS) mass spectrometry.[22−24] Systematic theoretical investigations using ab initio calculations designed to understand the reactivity of transition-metal cations with water have been reported by Ugalde et al.[25] These authors have addressed quantum mechanical constraints introduced by spin-forbidden crossings of the potential energy surfaces that are involved in the formation of oxide cations in the reactions of water with Sc^+ and V^+,[26] Cr^+,[27] Mn^+,[27] Fe^+,[27,28] Co^+, Ni^+, and Cu^+.[25] Similar surface crossings have been predicted very recently for the reaction of W^+ with water.[29] As far as we are aware, with the exception of the reaction with Hf^+,[30] none of the reactions of water with the atomic metal cations from the fifth and sixth row of the periodic table appears to have been studied previously.

In the measurements reported here, fourth-period atomic cations from K^+ to Se^+, fifth-period atomic cations from Rb^+ to Te^+ (excluding Tc^+), and sixth-period atomic cations from Cs^+ to Bi^+ were generated in one source, an ICP, which has been found to be suitable for virtually any element on the periodic table (with the exception of ions with a mass less than Ar).[31]

Higher-order chemistry initiated by the primary reactions of the atomic metal cations also can be monitored with the ICP/SIFT technique. In the experiments reported here with D_2O, the primary MO^+ product ions reacted further with D_2O to form MO_2^+ or MO_2D^+ or simply hydrate with D_2O. These observations of higher-order chemistry also will be reported.

2. Experimental Procedures

The experimental results reported here were obtained with the SIFT tandem mass spectrometer described in detail elsewhere.[32,33] This instrument was modified to accept ions generated in an ICP torch (ELAN series, PerkinElmer SCIEX) through an atmosphere−vacuum interface. The ICP ion source and interface have also been described previously,[31,34] as has the preparation of the solutions containing the atomic salt of interest that were peristaltically pumped via a nebulizer into the plasma.[5]

Atomic ions emerge from the ICP at a nominal ion temperature of 5500 K with corresponding Boltzmann state distributions. These distributions have been derived from available optical spectra[35,36] and reported by us previously for the two electronic spin states with the highest population at 5500 K.[4] Energy levels as high as 3.7 eV (3×10^4 cm^{-1}) were included in the calculations. The calculations show that excited states of the main-group elemental cations except Ba^+ are high in energy and contribute little (never more than 10%) to the total ion population at 5500 K. The ground ^2S state of Ba^+ contributes 44% and the excited ^2D state 55% at 5500 K. The state distributions are more variable for the transition-metal cations. The excited states at 5500 K contribute 20% or less toward the populations of Cr^+, Mn^+, Ni^+, Cu^+, Zn^+, Rh^+, Pd^+, Ag^+, Cd^+, Re^+, Au^+, and Hg^+ and 50% or more toward the populations of Ti^+, Y^+, Zr^+, Nb^+, La^+, and Ir^+ with Sc^+, V^+, Fe^+, Co^+, Mo^+, Ru^+, Hf^+, Ta^+, W^+, and Pt^+ having intermediate distributions at 5500 K, with Os^+ not known.

The ions emerging from ICP are injected through a differentially pumped sampling interface into a quadrupole mass spectrometer and, after mass analysis, introduced through an aspirator-like interface into flowing helium carrier gas at 0.35 ± 0.01 Torr and 295 ± 2 K. The ions are allowed to react with added D_2O a few milliseconds downstream of the flow tube.

After extraction from the ICP, the plasma ions may experience both radiative electronic-state relaxation and collisional electronic-state relaxation. The latter may occur already with argon as the extracted plasma cools upon sampling and then by collisions with He atoms in the flow tube (ca. 4×10^5 collisions with He) prior to the reaction region, but the actual extent of electronic relaxation (either radiative or collisional) is not known and is difficult to assess. Almost all of the electronic states of the transition-metal ions have positive parity; electric dipole transitions between states of the same parity are forbidden (Laporte rule).[37] This means that radiative transitions between different states in metal cations can be achieved only by either magnetic dipole or electric quadrupole radiation. The probabilities for these transitions are very low, and the resulting radiative lifetimes are of the order of seconds or larger. The time interval in the ICP-SIFT experiments between the exit of the ICP source and the entrance in the reaction region is ca. 20 ms, and therefore, no major modification of state distributions can occur in this time interval by forbidden radiative decay. That having been said, there were no indications of excited-state effects in our previous measurements of reactions of N_2O with atomic cations derived from the same ICP source operated in the same manner, except with Pt^+.[4] The many collisions experienced by the atomic cations with the quite polarizable Ar atoms as they emerge from the ICP and the ca. 4×10^5 collisions with He atoms in the flow tube (the helium buffer gas pressure was 0.35 ± 0.01 Torr) appear to be sufficient to provide for the thermalization of the excited states and ensure that the atomic ions reach a translational temperature equal to the tube temperature of 295 ± 2 K prior to entering the reaction region. However, the exact extent of electronic relaxation is uncertain. Clues to the presence of excited electronic states of the atomic ions in the reaction region can be found in the product ions observed and the shape of the semilogarithmic decay of the reacting atomic ion upon the addition of a neutral reactant. Curvature will appear in the measured atomic ion decay when the ground state and excited state react at different rates even when they give the same product ions. An excited-state effect cannot be seen when the products and reaction rates are the same for both the ground and the excited states, but in this case, the measured atomic ion decay defines the ground-state kinetics. Our growing experience has shown that excited states can reveal themselves when the ground state of the atomic ion reacts only slowly by termolecular addition and when excited states react rapidly in a bimolecular fashion. Our previous studies indicate that that the collisions with Ar and He ensure that most atomic ions reach a translational and internal temperature equal to the tube temperature of 295 ± 2 K prior to entering the reaction region.[1−6,38,39]

Reactant and product ions were sampled still further downstream with a second quadrupole mass spectrometer and were measured as a function of added reactant. The resulting profiles provide information about product ion distributions, reaction rate coefficients, and reaction molecularity. Rate coefficients for the primary bimolecular ion−molecule reactions are determined from the rate of decay of the reactant ion intensity with

TABLE 1: O-Atom Affinities ($D_0(M^+-O)$ (kcal mol^{-1})) and Ionization Energies (IE(M) (eV))[40] for Fourth-, Fifth-, and Sixth-Row Atomic Cations

M^+	$OA(M^+)$	IE(M)	M^+	$OA(M^+)$	IE(M)	M^+	$OA(M^+)$	IE(M)
K^+	3[a]	4.34	Rb^+	7[a]	4.18	Cs^+	14[a]	3.89
Ca^+	77.2[a]	6.11	Sr^+	71.4[a]	5.70	Ba^+	92.8[a]	5.21
Sc^+	164.6 ± 1.4[b]	6.56	Y^+	167.0 ± 4.2[c]	6.22	La^+	206 ± 4[d]	5.58
Ti^+	158.6 ± 1.6[b]	6.83	Zr^+	178.9 ± 2.5[c]	6.63	Hf^+	173 ± 5[a]	6.83
V^+	134.9 ± 3.5[b]	6.75	Nb^+	164.4 ± 2.5[c]	6.76	Ta^+	188 ± 15[a]	7.55
Cr^+	85.8 ± 2.8[b]	6.77	Mo^+	116.7 ± 0.5[c]	7.09	W^+	166 ± 10[f]	7.86
Mn^+	68.0 ± 3.0[b]	7.43	Tc^+			Re^+	115 ± 15[g]	7.83
Fe^+	80.0 ± 1.4[b]	7.90	Ru^+	87.9 ± 1.2[e]	7.36	Os^+	100 ± 12[h]	8.44
Co^+	74.9 ± 1.2[b]	7.88	Rh^+	69.6 ± 1.4[e]	7.46	Ir^+	59[a]	8.97
Ni^+	63.2 ± 1.2[b]	7.64	Pd^+	33.7 ± 2.5[e]	8.34	Pt^+	77,[i] 75 ± 2[j]	8.96
Cu^+	37.4 ± 3.5[b]	7.72	Ag^+	28.4 ± 1.2[e]	7.58	Au^+		9.23
Zn^+	38.5 ± 1.2[b]	9.39	Cd^+		8.99	Hg^+		10.44
Ga^+	5.6[a]	6.00	In^+		5.79	Tl^+		6.11
Ge^+	81.8[a]	7.90	Sn^+	75.1[a]	7.34	Pb^+	53.2[a]	7.42
As^+	147 ± 2[k]	9.81	Sb^+		8.64	Bi^+	41.6[a]	7.29
Se^+	92[k]	9.75	Te^+	96.6[a]	9.01	Po^+		

[a] Reference 51. [b] Reference 52. [c] Reference 53. [d] Reference 55. [e] Reference 54. [f] Reference 59. [g] Reference 56. [h] Reference 57. [i] Reference 58. [j] Reference 60. [k] Reference 4.

TABLE 2: OH Affinities of Bare Metal Cations ($D_0(M^+-OH)$ (kcal mol^{-1}))[a]

M^+	$D_0(M^+-OH)$	M^+	$D_0(M^+-OH)$	M^+	$D_0(M^+-OH)$
Ca^+	106	Sc^+	87.8	Mn^+	82
Sr^+	105 ± 5[b]	Ti^+	113	Fe^+	85.3
Ba^+	127 ± 7[b]	V^+	107	Co^+	72.2
Zn^+	30.4	Cr^+	74.3	Ni^+	42.2

[a] With a few exceptions, the values for $D_0(M^+-OH)$ were taken from ref 9. [b] Determined form ΔH_f° found in ref 51.

TABLE 3: H-Atom Affinities ($HA(M^+)$) of Bare Metal Cations ($HA(M^+) = D_0(M^+-H)$ (kcal mol^{-1}))[a]

M^+	$HA(M^+)$	M^+	$HA(M^+)$	M^+	$HA(M^+)$
		Ba^+	50.9[b]		
Sc^+	56.2 ± 2.2	Y^+	61.2 ± 1.9	La^+	57.1 ± 2.2
Ti^+	53.3 ± 2.6	Zr^+	52.1 ± 1.9	Hf^+	54.9[b]
					45.4 ± 2.5[c]
V^+	47.3 ± 1.4	Nb^+	52.6 ± 1.7	Ta^+	52.3 ± 1.2
Cr^+	31.5 ± 2.2	Mo^+	39.7 ± 1.4	W^+	55.0 ± 1.4
Mn^+	47.6 ± 3.4	Tc^+	50.7[d]	Re^+	44.5[b]
					52.8 ± 1.6[e]
Fe^+	48.8 ± 1.4	Ru^+	37.3 ± 1.2	Os^+	56.2[b]
Co^+	45.7 ± 1.4	Rh^+	38.5 ± 1.0	Ir^+	65.8[b]
					71.9 ± 1.4[f]
Ni^+	38.7 ± 1.9	Pd^+	47.8 ± 1.0	Pt^+	64.8 ± 1.2
Cu^+	21.0 ± 3.1	Ag^+	9.6 ± 1.4	Au^+	33.4[b]
					50.0 ± 1.8[g]
Zn^+	54.5 ± 3.1	Cd^+	42[b]	Hg^+	48.6[b]

[a] With few exceptions, the values for $HA(M^+)$ were taken from the review of ref 61. [b] Reference 63. [c] Reference 64. [d] Reference 62. [e] Reference 65. [f] Reference 66. [g] Reference 67.

an uncertainty estimated to be less than ±30%.[32,33] The uncertainty may be somewhat larger for slow reactions for which the measured decay is significantly less than an order of magnitude. Often, slow adduct formation is observed exclusively, and this can introduce curvature into the primary ion decay due to the occurrence of the reverse reaction (the extent of curvature will depend on the strength of the adduct bond being formed). Weak adduct bonding can lead to early curvature in the ion decay and so prevent the proper definition of the forward rate coefficient; only the determination of a lower limit to the rate coefficient is possible under such conditions. The approach to equilibrium can be monitored with a plot of the ratio of the concentration of the adduct ion over that of the bare ion against the flow of the added reactant. This ratio will curve upward as equilibrium is approached and increase linearly with flow when equilibrium is achieved. Linearity in the ratio plot provides a measure of the equilibrium constant, K, and so the standard free energy change, ΔG°_T, for the addition reaction since $\Delta G^\circ_T = -RT \ln K$. D_2O was introduced into the reaction region of the SIFT as a dilute mixture in helium (~2.5%) and was obtained commercially with high purity (Aldrich, isotopic purity >99.75%).

TABLE 4: Sequential Binding Energies for $M^+(H_2O)_n$ ($n \leq 4$) (kcal mol^{-1})[a]

M^+	**1**	**2**	**3**	**4**
K^+	17.9[b]	16.1[b]	13.2[b]	11.8[b]
Ca^+	28[c]	24[c]	21.5[c]	18.7[c]
Sc^+	34.5[d]	31.4[d]		
Ti^+	37.7 ± 1.4	32.6 ± 1.2	16.6 ± 1.6	19.9 ± 1.8
V^+	35.8 ± 1.2	36.0 ± 2.3	16.2 ± 1.1	16.0 ± 1.8
Cr^+	31.7 ± 2.1	34.0 ± 1.8	12.1 ± 1.2	12.1 ± 1.4
Mn^+	29.1 ± 1.4	21.5 ± 1.2	25.9 ± 1.4	11.8 ± 1.2
Fe^+	31.5 ± 1.2	39.3 ± 1.0	18.3 ± 0.9	11.8 ± 1.6
Co^+	39.3 ± 1.4	38.8 ± 1.6	15.5 ± 1.1	13.7 ± 1.4
Ni^+	43.9 ± 0.8	40.2 ± 1.8	16.2 ± 1.5	12.3 ± 1.5
Cu^+	38.4 ± 1.8	40.7 ± 1.6	13.7 ± 1.8	12.8 ± 1.0
Zn^+	32.5[d]	22.2[d]		
Rb^+	15.2[e]	13.5[e]	12.8[e]	12.8[e]
Sr^+	34.5[f]	30.5[f]	25.7[f]	22.3[f]
Cs^+	13.8[e]	11.8[e]	12.0[e]	14.7[e]
Ag^+	32.0 ± 1.9[g]	30.4 ± 1.9[g]	15.1 ± 2.2[g]	12.1 ± 2.9[g]
Au^+	40.1 ± 2.3[h]	45.0 ± 2.5[h]	23.1 ± 4.6[h]	20.8 ± 4.6[h]
Pb^+	22.4[f]	16.9[f]	12.2[f]	10.8[f]

[a] Unless indicated otherwise, the values for the binding energies of $M^+(H_2O)_n$ ($n \leq 4$) are taken from ref 21. [b] Reference 22. [c] Reference 68. [d] Reference 69. [e] Reference 70. [f] Reference 71. [g] Reference 72. [h] Reference 73.

3. Results and Discussion

The reactions of D_2O were measured with 46 atomic metal cations, including 29 transition-metal and 17 main-group cations, at a helium buffer gas pressure of 0.35 ± 0.01 Torr and a temperature of 295 ± 2 K. Both the primary and the higher-order chemistry was monitored. The primary reactions exhibited a wide range in reactivity with measured rate coefficients from $<5 \times 10^{-13}$ (for K^+) to 9.5×10^{-10} cm^3 molecule^{-1} s^{-1} (for

TABLE 5: Rate Coefficients (cm^3 molecule^{-1} s^{-1}), Reaction Efficiencies (k/k_c), Primary Product Ions and Their Distributions, and Higher-Order Product Ions Measured for Reactions of Atomic Ions M^+ with D_2O in Helium at 0.35 ± 0.01 Torr and 295 ± 2 K Ordered According to Row in the Periodic Table

M^+	k[a]	k_c[b]	k/k_c	primary products	PD (%)[c]	higher-order product ions
K^+	$<5.0 \times 10^{-13}$	2.42×10^{-9}	$<2.1 \times 10^{-4}$			
Ca^+	2.7×10^{-12}	2.42×10^{-9}	1.1×10^{-3}	$Ca^+(D_2O)$	100	$Ca^+(D_2O)_2$
Sc^+	1.6×10^{-10}	2.37×10^{-9}	6.8×10^{-2}	ScO^+	100	$ScO^+(D_2O)_{1-5}$
Ti^+	4.1×10^{-11}	2.34×10^{-9}	1.8×10^{-2}	TiO^+	100	$TiO^+(D_2O)_{1-5}$
V^+	1.1×10^{-11}	2.32×10^{-9}	4.7×10^{-3}	VO^+	70	$VO^+(D_2O)_{1-3}$
				$V^+(D_2O)$	30	$V^+(D_2O)_{2,3}$
Cr^+	2.0×10^{-12}	2.32×10^{-9}	8.6×10^{-4}	$Cr^+(D_2O)$	100	
Mn^+	$<5.0 \times 10^{-13}$	2.30×10^{-9}	$<2.2 \times 10^{-4}$	$Mn^+(D_2O)$	100	
Fe^+	6.0×10^{-12}	2.29×10^{-9}	2.6×10^{-3}	$Fe^+(D_2O)$	100	$Fe^+(D_2O)_2$
Co^+	1.7×10^{-12}	2.28×10^{-9}	7.5×10^{-4}	$Co^+(D_2O)$	100	$Co^+(D_2O)_{2-4}$
Ni^+	1.7×10^{-12}	2.28×10^{-9}	7.5×10^{-4}	$Ni^+(D_2O)$	100	$Ni^+(D_2O)_{2,3}$
Cu^+	9.0×10^{-12}	2.26×10^{-9}	4.0×10^{-3}	$Cu^+(D_2O)$	100	$Cu^+(D_2O)_2$
Zn^+	7.0×10^{-12}	2.25×10^{-9}	3.1×10^{-3}	$Zn^+(D_2O)$	100	
Ga^+	$<5.0 \times 10^{-13}$	2.23×10^{-9}	$<2.2 \times 10^{-4}$			
Ge^+	$<5.0 \times 10^{-13}$	2.22×10^{-9}	$<2.2 \times 10^{-4}$			
As^+	8.1×10^{-12}	2.22×10^{-9}	3.6×10^{-3}	AsO^+	10	$AsO^+(D_2O)$
				$As^+(D_2O)$	90	$As^+(D_2O)_{2-3}$
Se^+	$<5.0 \times 10^{-13}$	2.20×10^{-9}	$<2.2 \times 10^{-4}$	$Se^+(D_2O)$		
Rb^+	4.6×10^{-12}	2.19×10^{-9}	2.1×10^{-3}	$Rb^+(D_2O)$	100	
Sr^+	3.0×10^{-12}	2.18×10^{-9}	1.4×10^{-3}	$SrOD^+$	50	
				$Sr^+(D_2O)$	50	
Y^+	9.5×10^{-10}	2.18×10^{-9}	0.44	YO^+	100	$YO^+(D_2O)_{1-5}$
Zr^+	7.4×10^{-10}	2.17×10^{-9}	0.34	ZrO^+	100	$ZrO_2D^+(D_2O)_{0-3}$
						$ZrO^+(D_2O)_{1-4}$
Nb^+	3.0×10^{-11}	2.17×10^{-9}	1.4×10^{-2}	NbO^+	95	$NbO_2^+(D_2O)_{0-4}$
						$NbO^+(D_2O)_{1-3}$
				$Nb^+(D_2O)$	5	$Nb^+(D_2O)_{2-4}$
Mo^+	2.2×10^{-11}	2.16×10^{-9}	1.0×10^{-2}	MoO^+	90	$MoO^+(D_2O)$
				$Mo^+(D_2O)$	10	$MoO_2^+Mo^+(D_2O)_2$
Ru^+	1.0×10^{-12}	2.16×10^{-9}	4.6×10^{-4}	$Ru^+(D_2O)$	100	$Ru^+(D_2O)_2$
Rh^+	3.3×10^{-12}	2.15×10^{-9}	1.5×10^{-3}	$Rh^+(D_2O)$	100	$Rh^+(D_2O)_{2-5}$
Pd^+	7.2×10^{-13}	2.15×10^{-9}	3.3×10^{-4}	$Pd^+(D_2O)$	100	$Pd^+(D_2O)_2$
Ag^+	7.0×10^{-13}	2.14×10^{-9}	3.3×10^{-4}	$Ag^+(D_2O)$	100	
Cd^+	$<5.0 \times 10^{-13}$	2.14×10^{-9}	$<2.3 \times 10^{-4}$			
In^+	$<5.0 \times 10^{-13}$	2.13×10^{-9}	$<2.3 \times 10^{-4}$			
Sn^+	$<5.0 \times 10^{-13}$	2.13×10^{-9}	$<2.3 \times 10^{-4}$			
Sb^+	$<5.0 \times 10^{-13}$	2.12×10^{-9}	$<2.3 \times 10^{-4}$			
Te^+	$<5.0 \times 10^{-13}$	2.12×10^{-9}	$<2.3 \times 10^{-4}$			
Cs^+	5.0×10^{-13}	2.11×10^{-9}	2.3×10^{-4}	$Cs^+(D_2O)$	100	
Ba^+	3.0×10^{-12}	2.11×10^{-9}	1.4×10^{-3}	$BaOD^+$	100	$BaOD^+(D_2O)$
La^+	3.0×10^{-10}	2.11×10^{-9}	0.14	LaO^+	80	$LaO^+(D_2O)_{1-5}$
				$LaOD^+$	20	$LaOD^+(D_2O)$
Hf^+	7.5×10^{-10}	2.08×10^{-9}	0.36	HfO^+	100	$HfO^+(D_2O)$
						$HfO_2D^+((D_2O)_{0-4}$
Ta^+	2.6×10^{-10}	2.07×10^{-9}	0.13	TaO^+	100	$TaO_2^+(D_2O)_{0-4}$
W^+	2.0×10^{-11}	2.07×10^{-9}	9.7×10^{-3}	WO^+	100	$WO_2^+(D_2O)_{0-5}$
Re^+	$<5.0 \times 10^{-13}$	2.07×10^{-9}	$<2.4 \times 10^{-4}$	$Re^+(D_2O)$	100	
Os^+	$<5.0 \times 10^{-13}$	2.07×10^{-9}	$<2.4 \times 10^{-4}$			
Ir^+	1.4×10^{-11}	2.07×10^{-9}	6.8×10^{-3}	$Ir^+(D_2O)$	100	$Ir^+(D_2O)_{2-5}$
Pt^+	4.7×10^{-12}	2.07×10^{-9}	2.3×10^{-3}	$Pt^+(D_2O)$	100	$Pt^+(D_2O)_2$
Au^+	5.8×10^{-12}	2.07×10^{-9}	2.8×10^{-3}	$Au^+(D_2O)$	100	$Au^+(D_2O)_2$
Hg^+	8.1×10^{-12}	2.06×10^{-9}	3.9×10^{-3}	$Hg^+(D_2O)$	100	$Hg^+(D_2O)_2$
Tl^+	$<5.0 \times 10^{-13}$	2.06×10^{-9}	$<2.3 \times 10^{-4}$			
Pb^+	$<5.0 \times 10^{-13}$	2.06×10^{-9}	$<2.3 \times 10^{-4}$			
Bi^+	1.3×10^{-12}	2.06×10^{-9}	6.3×10^{-4}	$Bi^+(D_2O)$	100	$Bi^+(D_2O)_2$

[a] Measured reaction rate coefficient with an estimated accuracy of ±30%. Rate coefficients with values of 5×10^{-12} cm^3 molecule^{-1} s^{-1} or less may have a higher uncertainty. [b] Calculated capture rate coefficient (see text). [c] PD = product distribution expressed as a percentage, with an estimated accuracy of ±10%.

Y^+). Three reaction channels were observed, and these are indicated in reaction 1.

$$M^+ + D_2O \rightarrow MO^+ + D_2 \quad (1a)$$

$$\rightarrow MOD^+ + D \quad (1b)$$

$$\rightarrow M^+(D_2O) \quad (1c)$$

The bimolecular channels correspond to O-atom transfer (channel 1a) and OD transfer (channel 1b). The O-atom affinity of D_2 to form heavy water, $OA(D_2)$, is 117.5 kcal mol^{-1},[40] while the DO−D bond energy of D_2O is 121.3 kcal mol^{-1}.[40] Available O-atom affinities (Table 1) indicate that only 11 O-atom transfer reactions are exothermic out of the 46 that are possible with the atomic cations investigated. Available OD affinities are listed in Table 2, and only Ba^+ has an affinity for OD, 127.4 kcal mol^{-1}, that is higher than the DO−D bond energy. H-atom affinities are available for most metal cations and are listed in Table 3. All these values are much lower than the DO−D bond energy of D_2O = 121.3 kcal mol^{-1},[40] which means that D-atom

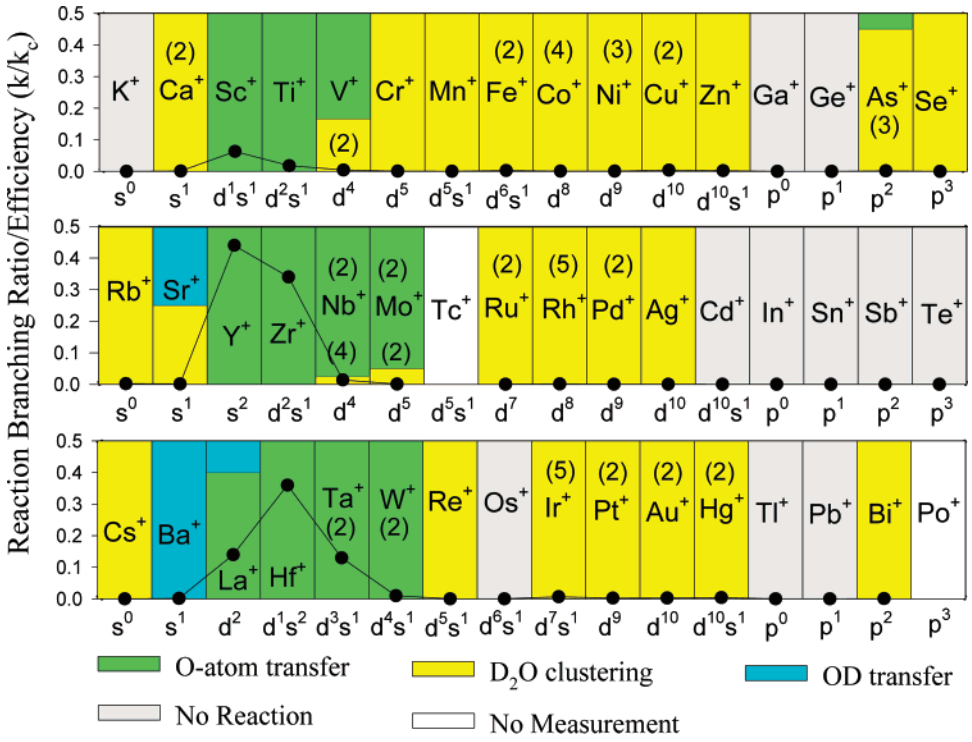

Figure 1. Periodic variations observed in the reaction efficiencies, k/k_c (solid circles), for reactions of atomic cations with D_2O. Measured reaction rate coefficient is represented by k, and k_c is the calculated collision rate coefficient (see text). Also indicated are the observed reaction channels and electronic configurations of atomic cations. Numbers in parentheses indicate the number of sequential events observed for the process indicated. The bar graphs indicate the reaction branching ratios and are scaled to 1.0 full scale.

transfer is endothermic with all of these atomic metal cations. Electron transfer was not observed to any of the 46 atomic cations since their recombination energies are much smaller than $IE(D_2O) = 12.6395 \pm 0.0003$ eV.[40] Channel 1c is assumed to occur in a termolecular reaction with helium acting as the third body that carries away the surplus energy in the reaction. Known sequential binding energies of $M^+(H_2O)_n$ ($n \leq 4$) are listed in Table 4.

Among the 46 atomic cations investigated, seven (Sc^+, Ti^+, Y^+, Zr^+, Hf^+, Ta^+, and W^+) exhibit the bimolecular channel 1a exclusively with measured rate coefficients in the range from 2.0×10^{-11} (for W^+) to 9.5×10^{-10} cm^3 molecule^{-1} s^{-1} (for Y^+), one cation (Ba^+) exhibits channel 1b exclusively with a rate coefficient of 3.0×10^{-12} cm^3 molecule^{-1} s^{-1}, and 21 cations exhibit only channel 1c with measured rate coefficients in the range from $<5 \times 10^{-13}$ (for K^+) to 1.4×10^{-11} cm^3 molecule^{-1} s^{-1} (for Ir^+). Eleven cations showed no products at all in the flow region investigated. Among the remaining six metal cations, four (V^+, As^+, Nb^+, and Mo^+) were observed to proceed by both channel 1a and channel 1c, one (La^+) by channels 1a and 1b, and one (Sr^+) by channels 1b and 1c. No attempt was made to measure the pressure dependence of channel 1c since a large range in pressure was not experimentally accessible. No obvious excited-state effects seemed present in the data. The semilogarithmic decays of the atomic ions Ti^+, Y^+, Zr^+, Nb^+, and Ir^+, all of which were calculated to have excited-state populations in the Ar plasma of $\geq$50%, did not exhibit obvious curvature (see Figures 2−4). The La^+ reaction did produce a minor (20%) channel that could not be unambiguously assigned to the La^+ (^{3}F, 5d^2) ground state as is discussed next (see section 3.5.).

Table 5 summarizes the measured rate coefficients, reaction efficiencies, observed primary products, and product distributions, as well as the observed higher-order products. The reaction efficiency is taken to be equal to the ratio of k/k_c, where k is the experimentally measured rate coefficient and k_c is the capture or collision rate coefficient computed using the algorithm of the modified variation transition-state classical trajectory theory developed by Su and Chesnavich[41] with $\alpha(D_2O) = 1.26 \times 10^{-24}$ cm^3,[42] and $\mu_d(D_2O) = 1.8545$ D.[43] Figure 1 displays the data in Table 5 and shows the overall trends in reaction efficiencies and primary product distributions on a periodic table.

3.1. Fourth-Row Atomic Ions. With the exception of the nonreaction of K^+, Ga^+, and Ge^+, only O-atom transfer and D_2O addition were observed as primary reaction channels for the fourth-row atomic metal cations. O-Atom transfer occurs with the very early transition-metal cations Sc^+ and Ti^+. D_2O addition was observed to compete with O-atom transfer to V^+ and the main-group cation As^+. The other fourth-row metal cations were observed to proceed only by D_2O addition.

Secondary and higher-order D_2O addition was observed with both MO^+ and $M^+(D_2O)$ ions as seen in Figure 2, which presents the data for Sc^+, Ti^+, Fe^+, and As^+. Higher-order D_2O addition according to reaction 2 was observed for the fourth row cations $M^+ = Ca^+$ ($n = 1$), V^+ ($n = 1$), Fe^+ ($n = 1$), Co^+ ($n = 1-3$), Ni^+ ($n = 1, 2$), Cu^+ ($n = 1$), and As^+ ($n = 1-2$). The Cr^+, Mn^+, Zn^+, and Se^+ cations only added one D_2O in the range of D_2O flow that was investigated. Reaction 3 was observed for $MO^+ = ScO^+$ ($n = 0-4$), TiO^+ ($n = 0-4$), VO^+ ($n = 0$), and AsO^+ ($n = 0$) in the range of D_2O flow that was investigated.

$$M^+(D_2O)_n + D_2O \rightarrow M^+(D_2O)_{n+1} \quad (2)$$

$$MO^+(D_2O)_n + D_2O \rightarrow MO^+(D_2O)_{n+1} \quad (3)$$

A rate coefficient for the reaction of Sc^+ with D_2O has been reported by Armentrout et al.[10] ($k = 1.3 \pm 0.4 \times 10^{-11}$ cm^3 molecule^{-1} s^{-1}), and the reactions of Ti^+ with H_2O and D_2O

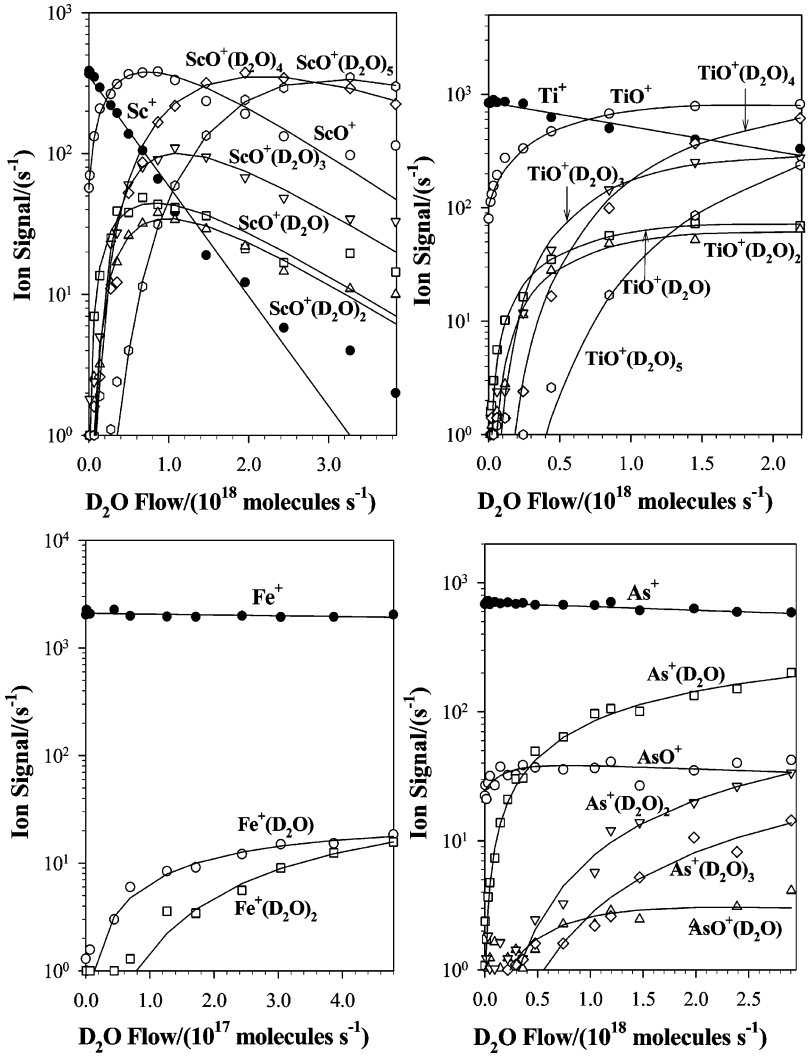

Figure 2. Composite of ICP/SIFT results for the reactions of the fourth-row metal cations Sc^+, Ti^+, Fe^+, and As^+ with D_2O in helium buffer gas at 0.35 ± 0.01 Torr and 295 ± 2 K.

have been measured by Castleman et al.[12,16] and Armentrout et al.[10] The Ti^+ results were somewhat controversial with suggestions that excited states might play a role. Our result for Ti^+ ($k = 4.1 \times 10^{-11}$ cm^3 molecule^{-1} s^{-1}) is in quite good agreement with Castleman's most recent flow reactor result obtained with H_2O in He buffer between 0.2 and 0.6 Torr ($k = 6.1 \times 10^{-11}$ cm^3 molecule^{-1} s^{-1}), but our results for Sc^+ and Ti^+ (1.8×10^{-10} and 4.1×10^{-11} cm^3 molecule^{-1} s^{-1}) are an order of magnitude larger than Armentrout's results ($k = 1.3 \pm 0.4 \times 10^{-11}$ and $3 \pm 1 \times 10-^{-12}$ cm^3 molecule^{-1} s^{-1}) obtained with D_2O at much lower pressures. There is no clear indication of a role for excited Sc^+ and Ti^+ states in our data shown in Figure 2, and the presence of excited states appears to have been ruled out for the low-pressure data. One reviewer suggests that the discrepancies in reaction rate coefficients may be a consequence of the difference in pressure (single vs multiple collisions), which may lead to a difference in the lifetime of the reaction intermediate against back dissociation due to the collisional quenching of the intermediate (with less back dissociation at higher pressures). However, this proposal is not supported by the pressure independence of the rate coefficient for the reaction of Ti^+ with H_2O in He buffer between 0.2 and 0.6 Torr observed by Castleman et al.[12] Also, the validity of extracting room-temperature rate coefficients from cross-sectional measurements at low energies under single-collision conditions as described by Chen et al.[10] may be questioned. The cross sections measured under single collision conditions apply to a reacting ion population that is not truly thermalized and does not have a Maxwell−Boltzmann population at a well-defined temperature; as such, the rate coefficients derived from these cross-sections are at best phenomenological.

The reaction of V^+ with D_2O has been measured previously by our group using ICP-SIFT ($k = 1.0 \pm 3.0 \times 10^{-11}$ cm^3 molecule^{-1} s^{-1})[14] and by Schwarz et al. using FTICR with H_2O ($k = 8.3 \pm 2.5 \times 10^{-12}$ cm^3 molecule^{-1} s^{-1}).[14] These results both are in line with our observation of slow VO^+ formation in the reaction with D_2O ($k = 1.1 \pm 3.0 \times 10^{-11}$ cm^3 molecule^{-1} s^{-1}). However, experiments by Armentrout's group with a flow tube ion source did not show a measurable formation of VO^+ from the reaction of ground-state $V^+(^5D)$ with D_2O, although the experimental results with a surface ionization source appear not to be as definitive about this nonreactivity.[18] Here, too, pressure effects may contribute to the apparent discrepancy.

We also have reported previously a nonreaction of Fe^+ with H_2O ($k < 1 \times 10^{-13}$ cm^3 molecule^{-1} s^{-1}), in which Fe^+ was produced by electronic impact on ferrocene and for which the addition of H_2O could not be demonstrated.[15] The previous rate coefficient of $<1 \times 10^{-13}$ cm^3 molecule^{-1} s^{-1} is much lower than that reported here, $k = 6 \times 10^{-12}$ cm^3 molecule^{-1} s^{-1}, although this value may well be an upper limit (see Figure 2). Also, the formation of some $Fe^+(D_2O)$ was observed in the experiments reported here (see Figure 2). The two results can

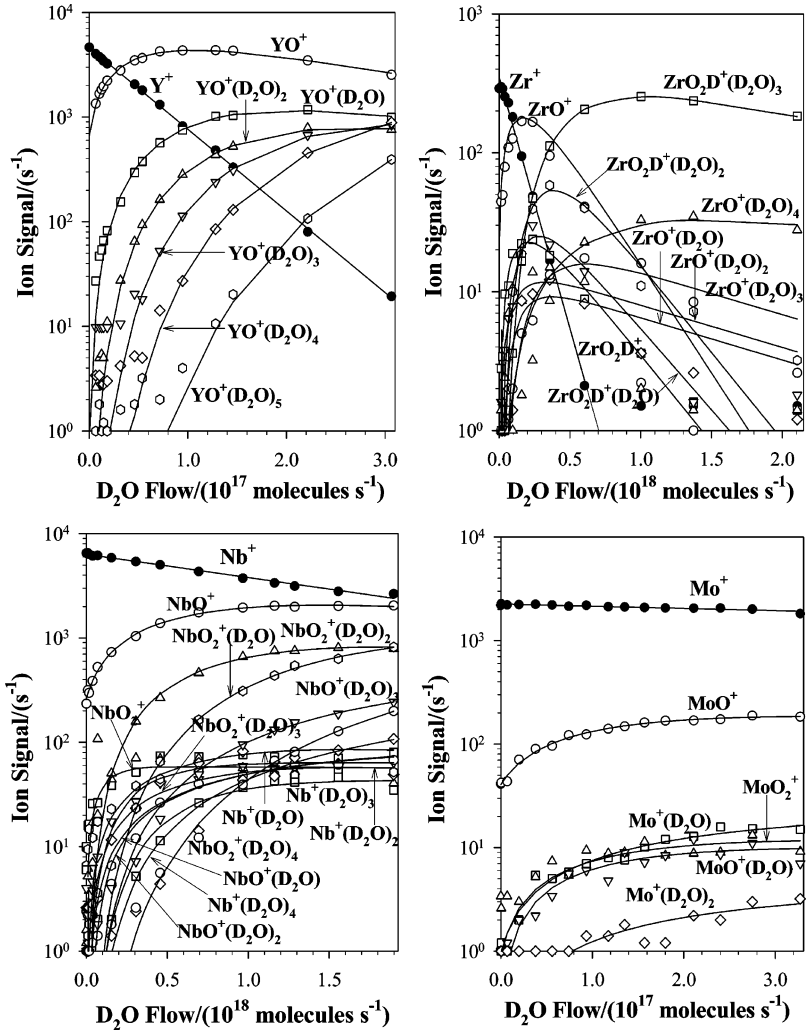

Figure 3. Composite of ICP/SIFT results for the reactions of the fifth-row metal cations Y^+, Zr^+, Nb^+, and Mo^+ with D_2O in helium buffer gas at 0.35 ± 0.01 Torr and 295 ± 2 K.

be brought in line if the water adduct in the earlier experiments was collisionally dissociated in the sampling process; less adduct formation would be observed, and the decay of the Fe^+ signal would be reduced with the resulting regeneration of Fe^+. The difference probably is too large to be attributed to a kinetic isotope effect.

3.2. Fifth-Row Atomic Ions. With the exception of the nonreactions with Cd^+, In^+, Sn^+, Sb^+, and Te^+ and the OD group transfer with Sr^+, O-atom transfer and D_2O addition also predominate in the reactions of the fifth-row metal cations with D_2O. O-Atom transfer was observed exclusively with Y^+ and Zr^+ and D_2O addition with Rb^+, Ru^+, Rh^+, Pd^+, and Ag^+. The D_2O addition was observed to compete with O-atom transfer to Nb^+ and Mo^+ and to compete with OD group transfer with Sr^+.

Figure 3 displays the primary and higher-order chemistry observed with Y^+, Zr^+, Nb^+, and Mo^+. The secondary O-atom transfer according to reaction 4 was observed for the metal cations $M^+ = Nb^+$ and Mo^+, and OD group transfer to metal oxides according to reaction 5 was observed for Zr^+.

$$MO^+ + D_2O \rightarrow MO_2^+ + D_2 \qquad (4)$$

$$MO^+ + D_2O \rightarrow MO_2D^+ + D \qquad (5)$$

Secondary and higher-order D_2O addition was observed with M^+, MO^+, MO_2^+, and MO_2D^+. Type 2 reactions were seen with $M^+ = Nb^+$ ($n = 1-3$), Mo^+ ($n = 1$), Ru^+ ($n = 1$), Rh^+ ($n = 1-4$), and Pd^+ ($n = 1$). Type 3 reactions were observed with $MO^+ = YO^+$ ($n = 0-4$), NbO^+ ($n = 0-2$), and MoO^+ ($n = 0$). Reactions 6 were observed with NbO_2^+ ($n = 0-3$). Reactions 7 were observed with ZrO_2D^+ ($n = 0-2$) and can be seen in Figure 3.

$$MO_2^+(D_2O)_n + D_2O \rightarrow MO_2^+(D_2O)_{n+1} \qquad (6)$$

$$MO_2D^+(D_2O)_n + D_2O \rightarrow MO_2D^+(D_2O)_{n+1} \qquad (7)$$

3.3. Sixth-Row Atomic Ions. With the exception of the nonreactions with Os^+, Tl^+, and Pb^+, and the OD group transfers with Ba^+ and La^+, O-atom transfer and D_2O addition are still the dominant reactions with the sixth-row metal cations. O-Atom transfer was observed exclusively with Hf^+, Ta^+, and W^+ and D_2O addition with Cs^+, Re^+, Ir^+, Pt^+, Au^+, Hg^+, and Bi^+. The O-atom transfer was observed to compete with the OD group transfer with La^+.

Figure 4 displays the primary and higher-order chemistry with Hf^+, Ta^+, W^+, and Ir^+. Secondary O-atom transfer according to reaction 4 was observed with $M^+ = Ta^+$ and W^+ to form TaO_2^+ and WO_2^+, respectively, and OD group transfer to metal oxide according to reaction 5 was observed with Hf^+ to form HfO_2D^+. Sequential D_2O addition was seen with all three of these secondary ions with the addition of up to four D_2O

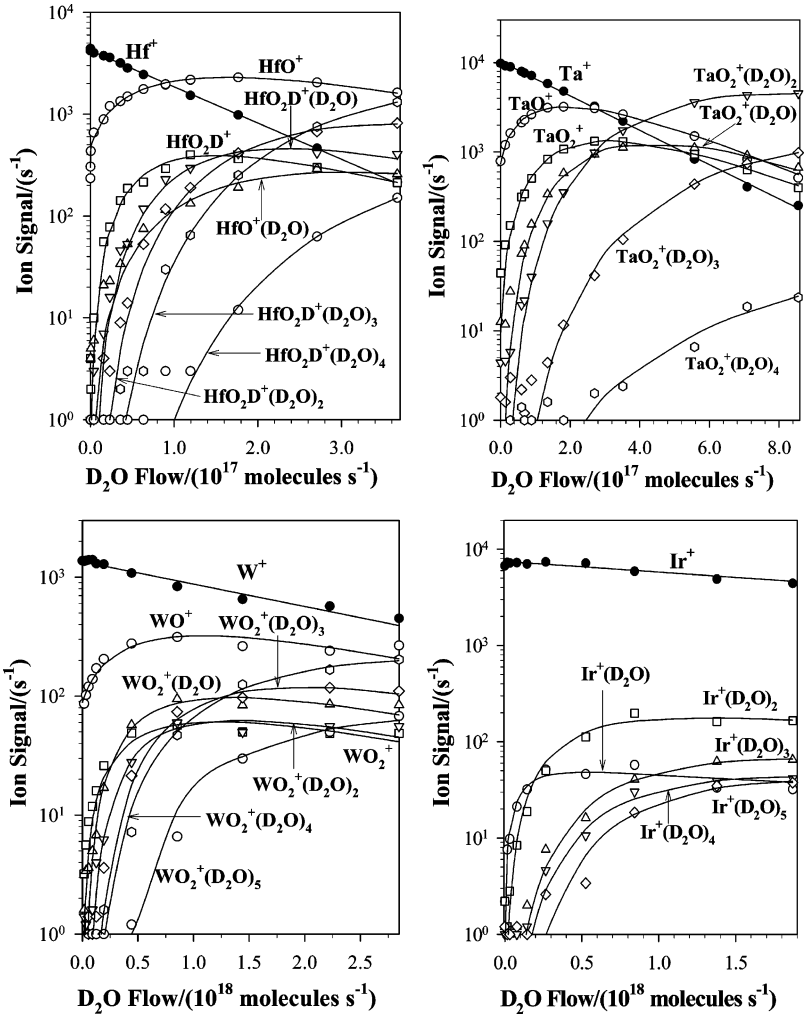

Figure 4. Composite of ICP/SIFT results for the reactions of the sixth-row metal cations Hf^+, Ta^+, W^+, and Ir^+ with D_2O in helium buffer gas at 0.35 ± 0.01 Torr and 295 ± 2 K.

molecules to form $HfO_2D^+(D_2O)_4$, $TaO_2^+(D_2O)_4$, and $WO_2^+(D_2O)_4$. Ir^+ is seen to add up to five D_2O molecules to form $Ir^+(D_2O)_5$. The faster second addition of D_2O to $Ir^+(D_2O)$ is clearly rate limited by its slower production from the addition of D_2O to Ir^+.

Secondary and higher-order D_2O addition is generally observed with the sixth-row metal species M^+, MO^+, MOD^+, MO_2^+, and MO_2D^+. Type 2 reactions were seen with $M^+ = Ir^+$ ($n = 1-4$), Pt^+ ($n = 1$), Au^+ ($n = 1$), Hg^+ ($n = 1$), and Bi^+ ($n = 1$). Type 3 reactions were seen with $MO^+ = LaO^+$ ($n = 0-4$) and HfO^+ ($n = 0$). Type 6 reactions were seen with $MO_2^+ = TaO_2^+$ ($n = 0-3$) and WO_2^+ ($n = 0-4$). Type 7 reactions were seen with $MO_2D^+ = HfO_2D^+$ ($n = 0-3$). Type 8 reactions were seen with $MOD^+ = BaOD^+$ ($n = 0$) and $LaOD^+$ ($n = 0$).

$$MOD^+(D_2O)_n + D_2O \rightarrow MOD^+(D_2O)_{n+1} \qquad (8)$$

Beauchamp and Irikura[30] previously investigated the reaction of Hf^+ with H_2O using FTICR with the ion produced by laser ablation of a metal foil, but their results are quite different from ours in that they show the two reaction channels of O-atom transfer and OH group transfer with a product distribution estimated as $I[HfO^+]/I[HfOD^+] = 1.6:1$ and a measured rate coefficient of 3.8×10^{-10} cm^3 molecule^{-1} s^{-1}. In comparison, our experiments indicate an exclusive O-atom transfer reaction channel with a larger rate coefficient of 7.5×10^{-10} cm^3 molecule^{-1} s^{-1}. If the OH transfer channel is due to the reaction of the low-lying ^4F excited-state of Hf^+, then the channel discrepancy may be due to a higher proportion of this state produced in the laser ablation of the Hf foil in the FTICR experiments. There is better agreement on the higher-order chemistry as both experiments show further reaction of HfO^+ to form $HfO_2H^+(HfO_2D^+)$ and then its hydrate, but our rate coefficient of 6.4×10^{-10} cm^3 molecule^{-1} s^{-1} for the reaction of HfO^+ is again larger than that of 1.6×10^{-10} cm^3 molecule^{-1} s^{-1} reported by Beauchamp and Irikura.[30]

3.4. O-Atom Transfer (Dehydrogenation). *3.4.1. Thermodynamics and Efficiency.* According to the O-atom affinities listed in Table 1, only metal cations in groups 3B to 6B have higher O-atom affinities than $OA(D_2) = 117.8 \pm 0.1$ kcal mol^{-1},[40] and this means that only these cations are thermodynamically allowed to abstract an O-atom from D_2O, viz. to cause dehydrogenation and release D_2. Indeed, only these metal cations were observed to dehydrogenate D_2O. Dehydrogenation was observed with the group 3B (Sc^+, Y^+, and La^+), group 4B (Ti^+, Zr^+, and Hf^+), group 5B (V^+, Nb^+, and Ta^+), and group 6B (Mo^+ and W^+) transition-metal cations and the main-group cation As^+. Rate coefficients for O-atom transfer are in the range of 8.1×10^{-13} (As^+) to 9.5×10^{-10} (Y^+) cm^3 molecule^{-1} s^{-1}. OD transfer was observed to compete with O-atom transfer in the reactions of La^+ (20%), and D_2O addition was observed to compete with O-atom transfer with V^+ (33%), As^+ (90%), Nb^+ (5%), and Mo^+ (10%).

Figure 5 displays the dependence of the efficiency of O-atom transfer on the known O-atom affinity of the metal cation. It is interesting to note in Figure 5 that O-atom transfer from D_2O to Mo^+ is slightly endothermic and almost thermoneutral, $\Delta H_{298} = 1.1 \pm 0.6$ kcal mol^{-1}. Also, given that O-atom transfer generally predominates when exothermic or nearly thermoneutral, we can assign an upper limit to OA(Re^+), OA(Re^+) < 117.8 kcal mol^{-1}, since only D_2O addition was observed with Re^+. This limit improves the value of OA(Re^+) = 115 ± 15 kcal mol^{-1} in Table 1 to 109 ± 9 kcal mol^{-1}.

3.4.2. Spin Control and Reaction Mechanism. Figure 5 shows that the reactions with D_2O often proceed with efficiencies below 0.1 when O-atom transfer is exothermic, even below 0.01 for the fourth-row atomic cations V^+ (0.0032) and As^+ (0.00036). Low efficiencies for exothermic O-atom transfer are interesting and, given our previous experience with O-atom transfer from N_2O to atomic cations,[4] are likely to speak to the role of electronic spin conservation in the formation of the monoxide cation. O-Atom transfer from D_2O is not overly exothermic, by less than 88 kcal mol^{-1}, as compared to O-atom transfer from N_2O that can be exothermic by as much as 168 kcal mol^{-1}.

We note, first of all, that the exothermic O-atom transfer reactions were observed to be inefficient (<0.1) in our experiments with D_2O, viz. the reactions of Sc^+ (0.068), Ti^+ (0.018), V^+ (0.0032), and As^+ (0.00036) in the fourth row, Nb^+ (0.013) and Mo^+ (0.0090) in the fifth row, and W^+ (0.0097) in the sixth row, where efficiencies for the O-atom transfer channel are given in parentheses. The one or two electronic states of these atomic cations with the highest population within the ICP are all high-spin states: $Sc^+(^3D, ^3F)$, $Ti^+(^4F)$), $V(^5D, ^5F)$, $Nb^+(^5D, ^5F)$, Mo^+-$(^6S, ^6D)$, and $W^+(^6D)$.[4] Their reactions with D_2O by O-atom transfer to produce metal−oxide cations in their ground states ($ScO^+(^1\Sigma)$, $TiO^+(^2\Delta)$, $VO^+(^3\Sigma)$, $NbO^+(^3\Sigma)$, $MoO^+(^4\Sigma)$, and $WO^+(^4\Sigma)$)[4] are all spin-forbidden (see reactions 9−14 for which the measured reaction efficiencies and reaction enthalpies in kcalories per mol are also indicated).

$$Sc^+(^3D, ^3F) + D_2O(^1A_1) \rightarrow ScO^+(^1\Sigma) + D_2(^1\Sigma_g^+) \quad 0.068 \quad -47 \quad (9)$$

$$Ti^+(^4F) + D_2O(^1A_1) \rightarrow TiO^+(^2\Delta) + D_2(^1\Sigma_g^+) \quad 0.018 \quad -41 \quad (10)$$

$$V^+(^5D, ^5F) + D_2O(^1A_1) \rightarrow VO^+(^3\Sigma) + D_2(^1\Sigma_g^+) \quad 0.0032 \quad -17 \quad (11)$$

$$Nb^+(^5D, ^5F) + D_2O(^1A_1) \rightarrow NbO^+(^3\Sigma) + D_2(^1\Sigma_g^+) \quad 0.013 \quad -47 \quad (12)$$

$$Mo^+(^6S, ^6D) + D_2O(^1A_1) \rightarrow MoO^+(^4\Sigma) + D_2(^1\Sigma_g^+) \quad 0.0097 \quad +1 \quad (13)$$

$$W^+(^6D) + D_2O(^1A_1) \rightarrow WO^+(^4\Sigma) + D_2(^1\Sigma_g^+) \quad 0.0097 \quad -48 \quad (14)$$

Apparently, the rates of these reactions are constrained by the change in spin required to proceed from the reactant to the product potential energy surfaces, as has been proposed previously by Armentrout et al.[10,18] for the reactions of Sc^+, Ti^+, and V^+.

The reaction of D_2O with As^+ may be a special case among the main-group atomic cations in that the ground-state O-atom transfer reaction 15 is exothermic, spin-forbidden and inefficient.

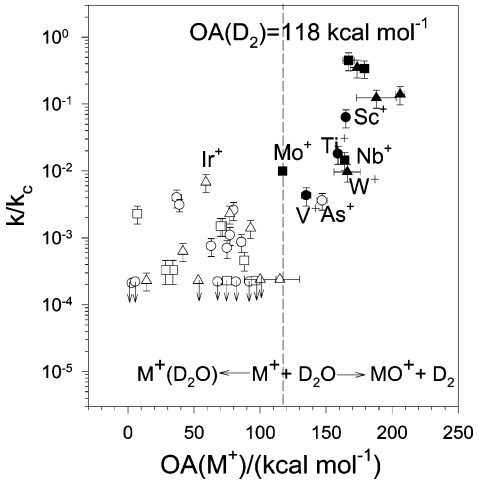

Figure 5. Dependence of the reaction efficiency, k/k_c, on the O-atom affinity, OA, of the atomic cation M^+. Measured reaction rate coefficient is represented by k, and k_c is the calculated collision rate coefficient. Reactions on the right of the dashed line are exothermic for O-atom transfer, while those on the left are endothermic. Circles refer to fourth-row cations, squares to fifth-row cations, and triangles to sixth-row cations. Open symbols designate the observation of D_2O addition, while solid symbols designate the observation of O-atom transfer.

$$As^+(^3P) + D_2O(^1A_1) \rightarrow AsO^+(^1\Sigma) + D_2(^1\Sigma_g^+) \quad 0.0036 \quad -29 \quad (15)$$

The appearance of small amounts of AsO^+ at low flows of D_2O recorded in Figure 2 may well be the result of the spin-allowed reaction of excited $As^+(^1D)$, which has been estimated to be formed in the Ar plasma at levels of ca. 6% of the total As^+ ion population.[4]

Other reactions that are spin-forbidden for the formation of ground-state products appear to be sufficiently exothermic to achieve a high reaction efficiency with the formation of spin-allowed excited products. These include the reactions with the high-spin states of $Y^+(^3D)$, $Zr^+(^4F)$, $La^+(^3F, ^3D)$, $Hf^+(^2D,^4F)$, and $Ta^+(^5F, ^3F)$, for which the monoxide cations have ground states of $YO^+(^1\Sigma)$, $ZrO^+(^2\Sigma)$, $LaO^+(^1\Sigma)$, $HfO^+(^2\Sigma)$, and TaO^+-$(^3\Delta)$.[4] However, collisional de-excitation to the ground state (e.g., $Y^+(^1S)$) or a low-lying state (e.g., $La^+(^1D)$) can promote spin-allowed O-atom transfer and so cannot be ruled out. In the case of Hf^+, the ground ^2D state is already sufficiently populated (48%)[11] within the ICP to possibly account for the observed O-atom transfer efficiency (0.36).

The potential-energy surface for the exothermic but spin-forbidden dehydrogenation of D_2O with ground-state $V^+(^5D)$ has been described previously by Armentrout et al.[18] and Ugalde et al.[26] The reaction path involves the initial formation of the ion dipole complex $V^+{\cdot}OD_2$, which then isomerizes by insertion to form D−V^+−OD, evolves through a four-centered transition state into $VO^+{\cdot}D_2$, and then separates into the products $VO^+(^3\Sigma) + D_2$. The overall transformation involves a crossing to a low-spin triplet state located between the intermediate D−V^{+-}OD and the $V^+{\cdot}OD_2$ complex and lies above the initial energy of the reactants.

Armentrout et al.[18] and Ugalde et al.[26] also have considered the mechanism for metal−oxide production in the reaction of D_2O with the ground states $Sc^+(^3D)$ and $Ti^+(^4F)$. The mechanisms are qualitatively similar to that proposed for the analogous

TABLE 6: Measured Equilibrium Constants (K) and Derived Standard Free Energy Changes ($\Delta G°$ (kcal mol^{-1})) for Sequential D_2O Addition to Metal Cations at 0.35 ± 0.01 Torr and 295 ± 2 K

	K ($\Delta G°$)		
M^+	$M^+(D_2O)$	$M^+(D_2O)_2$	$M^+(D_2O)_3$
Ca^+	$\geq 8.2 \times 10^4$ (≤ -6.7)	2.1×10^6 (-8.6)	
V^+	$\geq 6.7 \times 10^4$ (≤ -6.6)		
Cr^+	$\geq 3.1 \times 10^4$ (≤ -6.1)		
Mn^+	$\geq 1.7 \times 10^4$ (≤ -5.8)		
Fe^+	$\geq 2.2 \times 10^5$ (≤ -7.3)	$\geq 2.4 \times 10^7$ (≤ -10.1)	
Co^+	$\geq 1.0 \times 10^5$ (≤ -6.8)	$\geq 9.6 \times 10^6$ (≤ -9.5)	6.9×10^5 (-8.0)
Ni^+	$\geq 4.1 \times 10^5$ (≤ -7.6)	$\geq 2.3 \times 10^7$ (≤ -10.0)	1.4×10^7 (-9.8)
Cu^+	$\geq 4.1 \times 10^5$ (≤ -7.6)		
Zn^+	$\geq 1.3 \times 10^5$ (≤ -7.0)		
As^+	$\geq 1.2 \times 10^6$ (≤ -8.3)		
Sr^+	$\geq 2.0 \times 10^4$ (≤ -5.9)		
Mo^+	$\geq 7.3 \times 10^4$ (≤ -6.6)		
Ru^+	$\geq 2.5 \times 10^5$ (≤ -7.4)		
Rh^+	1.3×10^5 (-7.0)	4.5×10^6 (-9.1)	2.2×10^6 (-8.6)
Pd^+	$\geq 3.7 \times 10^4$ (≤ -6.2)	$\geq 1.1 \times 10^6$ (≤ -8.2)	
Ag^+	$\geq 1.0 \times 10^5$ (≤ -6.8)		
Cs^+	3.3×10^4 (-6.2)		
Ir^+	≥ -7.3 ($\leq 2.3 \times 10^5$)	2.3×10^7 (-10.2)	1.4×10^7 (-8.6)
Pt^+	$\geq 3.9 \times 10^4$ (≤ -6.3)		
Au^+	$\geq 1.8 \times 10^5$ (≤ -7.2)		
Hg^+	$\geq 7.9 \times 10^4$ (≤ -6.7)		
Bi^+	$\geq 2.1 \times 10^4$ (≤ -5.9)		

reaction with $V^+(^5D)$ and also involve crossings of different spin states. The exothermicities for oxide formation are in the order $Sc^+ > Ti^+ > V^+$ as are the efficiencies observed by us. All three reactions are spin-forbidden overall and relatively inefficient, 0.068 > 0.018 > 0.0031, for MO^+ formation. VO^+ formation is by far the least efficient of the three (6× less efficient than TiO^+ formation), is the only one of the three that competes with D_2O addition, and also is the only one for which calculations predict that the spin crossing lies above the energy of the high-spin reagents. The potential energy surface computed for exothermic WO^+ formation exhibits a low-lying sextet/quartet crossing and subsequent barrier on the quartet surface of only 5.1 kcal mol^{-1}, and this is consistent with the observed efficiency of 0.0097.

3.5. OD Transfer. Primary OD transfer was observed exclusively (100%) only in the reaction of Ba^+ with D_2O and competed with O transfer in the reaction with La^+ (20%) and with D_2O addition in the reaction with Sr^+ (50%).

The DO−D bond energy of D_2O is quite high, 121.3 kcal mol^{-1}.[40] Available OD affinities for atomic metal cations are listed in Table 2; they are known for only 12 of the 46 atomic cations that were investigated. Of these, only Ba^+ appears to have an affinity, $D_0(Ba^+-OD) > D(DO-D)$, with $D_0(Ba^+-OD) = 127 \pm 7$ kcal mol^{-1}. We did observe OD transfer in the reaction of Ba^+ with D_2O, but with a low efficiency of about 1.4×10^{-3}, perhaps due to a very slight endothermicity. The heavy hydroxide cation also was observed as a product in the reaction with Sr^+ but in this case in competition with adduct formation. In this case, however, we must attribute the heavy hydroxide formation to reaction with excited state $Sr^+(^2D, 4d)$ since $D_0(Sr^+-OD) = 105 \pm 5$ kcal mol^{-1} so that OD transfer is endothermic by at least 10 kcal mol^{-1} for the reaction with ground-state Sr^+. The maximum excited-state population of Sr^+ should be about 10%,[11] and this could easily account for the observed 50% occurrence of OD transfer. The OD affinity of La^+ appears not to be available but should be higher than $D(DO-D)$ for OD transfer to be exothermic with ground-state $La^+(^3F)$. In this case also, we cannot exclude the possible role of excited states such as $La^+(^1D, 5d6s)$, which contributes 11%, and $La^+(^3D)$, which contributes 23% in the ICP plasma at 5500 K.[11] These two states both have s^1 orbitals available for bonding as is the case of Sr^+ and Ba^+.[4]

The OD transfer channel was easily observed by Armentrout et al.[10,17,18,44] in reactions of the fourth-row transition-metal cations with D_2O at the higher energies available in a guided ion beam instrument. All the OD transfer reactions were found to be endothermic at room temperature and so are expected not to be observed in our ICP/SIFT instrument. Studies of the reactions of Ba^+, Sr^+, and La^+ with D_2O were not reported.

3.6. D_2O Addition (Hydration). Addition of D_2O was observed exclusively in the reactions of the fourth-row cations Ca^+, Mn^+, Fe^+, Co^+, Ni^+, Cu^+, Zn^+, and Se^+, the fifth-row cations Rb^+, Ru^+, Rh^+, Pd^+, and Ag^+, and the sixth-row cations Cs^+, Re^+, Ir^+, Pt^+, Au^+, Hg^+, and Bi^+. Beside these, D_2O addition was observed to compete with O-atom transfer in the ractions with V^+, As^+, Nb^+, and Mo^+ and to compete with OD group transfer in the reactions with Sr^+. All these addition reactions are presumed to occur by the collisional stabilization reaction 16 at 0.35 Torr of He (however, pressure-dependent studies were not performed).

$$M^+ + D_2O + He \rightarrow M^+ D_2O + He \qquad (16)$$

D_2O addition reactions were observed to proceed with relatively small effective bimolecular rate coefficients, $k \leq 1.4 \times 10^{-11}$ cm^3 molecule^{-1} s^{-1}, presumably due the short lifetime of the intermediate complex that is expected from the weak bonding of the atomic ion with water and the small degrees of freedom available for energy partitioning. No products at all were observed in the reactions of K^+, Ga^+, Ge^+, Cd^+, In^+, Sn^+, Sb^+, Te^+, Os^+, Tl^+, and Pb^+ with D_2O.

Two D_2O molecules were observed to add sequentially to the first-row cations Ca^+, Fe^+, and Cu^+, the second-row cations Mo^+, Ru^+, and Pd^+, and the third-row cations Pt^+, Au^+, Hg^+, and Bi^+. V^+, Ni^+, and As^+ were observed to add three D_2O molecules. Co^+ and Nb^+ were observed to add four D_2O molecules, and only Ir^+ and Rh^+ were observed to add five D_2O molecules in the D_2O flow range that was investigated.

In general, the higher-order rate coefficients for addition are higher than the primary ones, and this can be attributed to the increased number of degrees of freedom in the higher-order reaction intermediates, which leads to longer lifetimes and so higher rates of collisional stabilization. Furthermore, the second water molecule often binds as strongly as, or more strongly than,[9,45,46] the first (see Table 4), and this is also kinetically favorable for water addition since the lifetime of the intermediate also increases with increasing binding energy.

Equilibrium analyses were performed on the kinetic results by plotting product/reactant ion signal ratios as a function of reactant flow. Equilibrium is achieved when such a plot achieves linearity, viz. when $[M^+(D_2O)_n]/[M^+(D_2O)_{n-1}] = K_{eq}$ $[D_2O]$. The equilibrium analyses show that equilibrium was not achieved with most cations, and so most of the reported values for K_{eq} are lower limits. Calculated equilibrium constants, K_{eq}, and the corresponding changes in standard free energy, $\Delta G°$, are presented in Table 6. The apparent bimolecular efficiencies for hydration are presented in Table 7. According to the formula $\Delta G° = \Delta H° - T\Delta S°$ and that $\Delta S°$ for all the metal cations clustering with D_2O is nominally 20 eu,[22,47] there is a constant difference of about 6 kcal mol^{-1} between $\Delta G°$ and $\Delta H°$ at 298 K. For certain cations, we can make sure that equilibrium has been achieved, and the values for $\Delta G°$ in Table 6 can agree with the values of $\Delta H°$ in Table 4. For example, for Cs^+, the

TABLE 7: Measured Reaction Rate Coefficients (k^a (cm^3 $molecule^{-1}$ s^{-1})) and Reaction Efficiencies (k/k_c) for Sequential D_2O Addition to M^+ in Helium at 0.35 ± 0.01 Torr and 295 ± 2 K

	$M^+(D_2O)$		$M^+(D_2O)_2$		$M^+(D_2O)_3$	
M^+	k	k/k_c	k	k/k_c	k	k/k_c
Ca^+	2.7×10^{-12}	1.1×10^{-3}	1.3×10^{-10}	5.7×10^{-2}		
V^+	3.3×10^{-12}	1.4×10^{-3}				
Cr^+	2.0×10^{-12}	8.6×10^{-4}				
Mn^+	$<5.0 \times 10^{-13}$	$<2.2 \times 10^{-4}$				
Fe^+	6.0×10^{-12}	2.6×10^{-3}	9.0×10^{-11}	4.1×10^{-2}		
Co^+	1.7×10^{-12}	7.5×10^{-4}	2.6×10^{-10}	0.12	2.7×10^{-10}	0.13
Ni^+	1.7×10^{-12}	7.5×10^{-4}	2.8×10^{-10}	0.13		
Cu^+	9.0×10^{-12}	4.0×10^{-3}	3.2×10^{-11}	1.5×10^{-2}		
Zn^+	7.0×10^{-12}	3.1×10^{-3}				
As^+	7.3×10^{-12}	3.2×10^{-3}	2.6×10^{-11}	1.2×10^{-2}		
Sr^+	1.6×10^{-12}	7.0×10^{-4}				
Mo^+	2.2×10^{-12}	1.0×10^{-3}				
Ru^+	1.0×10^{-12}	4.6×10^{-4}				
Rh^+	3.3×10^{-12}	1.5×10^{-3}	5.8×10^{-11}	2.7×10^{-2}		
Pd^+	7.2×10^{-13}	3.3×10^{-4}	5.6×10^{-11}	2.6×10^{-2}		
Ag^+	7.0×10^{-13}	3.3×10^{-4}				
Cs^+	5.0×10^{-13}	2.4×10^{-4}				
Ir^+	1.4×10^{-11}	6.8×10^{-3}	3.0×10^{-10}	0.15		
Pt^+	4.7×10^{-12}	2.3×10^{-3}				
Au^+	5.8×10^{-12}	2.8×10^{-3}	2.1×10^{-10}	0.10		
Hg^+	8.0×10^{-12}	3.9×10^{-3}	4.8×10^{-11}	2.3×10^{-2}		
Bi^+	1.3×10^{-12}	6.2×10^{-4}				

[a] Effective bimolecular rate coefficient with an estimated accuracy of ±50%.

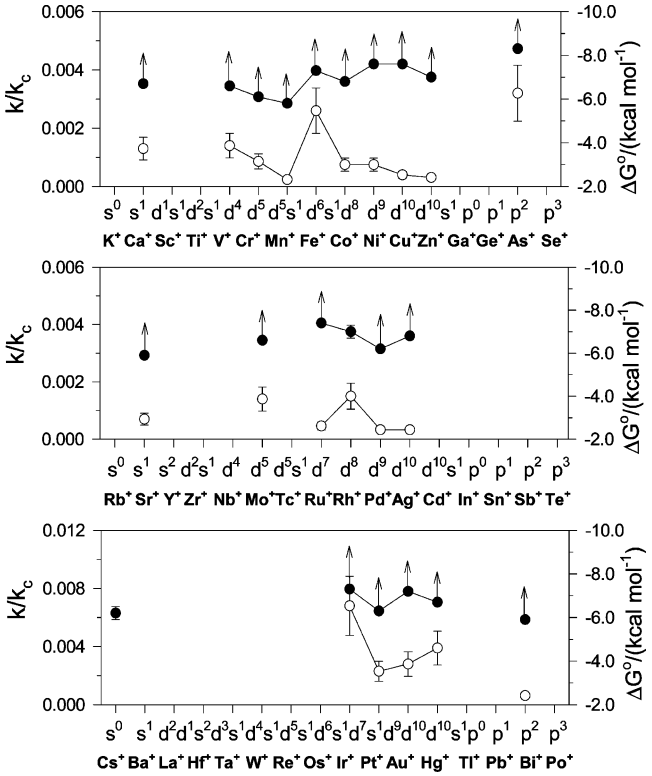

Figure 6. Variations in the reaction efficiency, k/k_c (open circles), and standard free energy change, $\Delta G°$ (solid circles), for single D_2O addition to bare first-, second-, and third-row atomic metal cations at room temperature.

value of $\Delta H°$ in our experiment is about 12.1 kcal mol^{-1} based on $\Delta S° = 19.4$ eu,[22] which is in good agreement with the value 12.9 kcal mol^{-1} in Table 4. Figure 6 explores the periodic variation in the values of the measured efficiencies and the standard binding free energies observed from our equilibrium measurements (see Table 6) for the addition of D_2O to M^+ at 295 ± 2 K.

D_2O addition was also observed with many of the MO^+, MOD^+, MO_2^+, and MO_2D^+ cations that were formed in the reactions of the early transition-metal ions. Up to five D_2O molecules were observed to add sequentially to MO^+ and MO_2^+, four to MO_2D^+, and one with MOD^+ (see Table 5).

3.7. MO_2^+ and MO_2D^+ Formation. A second O-atom transfer, reaction 4, was observed with the early transition-metal oxides NbO^+, MoO^+, WO^+, and TaO^+, and OD group transfer, reaction 5, was observed with ZrO^+ and HfO^+. The rate coefficients measured for these reactions are summarized in Table 8 along with calculated reaction efficiencies. O-Atom transfer to TaO^+ is the most efficient secondary O-atom transfer, $k/k_c = 0.14$, and that to NbO^+ is the least, $k/k_c = 0.020$. The OD group transfer reactions with HfO^+ and ZrO^+ are both quite efficient with k/k_c equal to 0.31 and 0.12, respectively.

Available O-atom affinities for atomic metal oxide cations are listed in Table 9. Of these, five (those for the early transition-metal oxide cations NbO^+, MoO^+, TaO^+, and WO^+ and the late transition−-metal oxide cation IrO^+) have $OA(MO^+) > OA(D_2)$. We observed O-atom transfer with all four of the early transition-metal oxide cations but could not investigate this reaction with IrO^+. This latter ion was not generated in the reaction of Ir^+ with D_2O since only in this interesting case was $OA(M^+) < OA(D_2)$, while $OA(MO^+) > OA(D_2)$.

The structure of the MO_2^+ ions formed in reaction 4 is uncertain. Our multi-collision induced dissociation technique,[48] which involves simply raising the potential of the sampling nose cone, did not yield bond cleavage for MO_2^+ and so did not provide bond connectivity information. But, based on the elemental composition, three different bonding isomers are possible: the end-on metal dioxygen complex I, MOO^+, the side-on complex II, c-MO_2^+, and the inserted metal dioxide complex III, OMO^+. Several of these isomers may even coexist for some of these metals. For example, structures I and III were computed to coexist as well-separated minima on different spin surfaces of CrO_2^+.[49] A general guide has been provided by Schwarz et al.,[50] who propose that structure III is energetically

TABLE 8: Rate Coefficients (cm^3 $molecule^{-1}$ s^{-1}) Measured for O-Atom Transfer and OD Transfer Reactions of Metal Oxide Cations with D_2O in Helium at 0.35 ± 0.01 Torr and 295 ± 2 K

reaction	k^a	k_c	k/k_c
$NbO^+ + D_2O \rightarrow NbO_2^+ + D_2$	4.3×10^{-11}	2.17×10^{-9}	0.020
$MoO^+ + D_2O \rightarrow MoO_2^+ + D_2$	2.2×10^{-10}	2.17×10^{-9}	0.10
$TaO^+ + D_2O \rightarrow TaO_2^+ + D_2$	3.0×10^{-10}	2.09×10^{-9}	0.14
$WO^+ + D_2O \rightarrow WO_2^+ + D_2$	6.0×10^{-11}	2.09×10^{-9}	0.029
$HfO^+ + D_2O \rightarrow HfO_2D^+ + D$	6.4×10^{-10}	2.10×10^{-9}	0.31
$ZrO^+ + D_2O \rightarrow ZrO_2D^+ + D$	2.6×10^{-10}	2.17×10^{-9}	0.12

[a] Reaction rate coefficient with an estimated accuracy of ±30%.

TABLE 9: O-Atom Affinities of Atomic Metal Oxide Cations ($D_0(MO^+-O)$ (kcal mol^{-1}))[a]

MO^+	$OA(MO^+)$	MO^+	$OA(MO^+)$	MO^+	$OA(MO^+)$
ScO^+	40	YO^+	41	LaO^+	23
TiO^+	81	ZrO^+	89		
VO^+	90	NbO^+	132	TaO^+	140
CrO^+	66	MoO^+	128	WO^+	132
FeO^+	66	RuO^+	79	ReO^+	65
CuO^+	99	RhO^+	78	OsO^+	105
				IrO^+	125
				PrO^+	75

[a] Reference 50.

favored for low oxidation states as well as those metals that have a preference for the formation of high-valent oxides, while structures I and II prevail for the late transition metals that do not support high oxidation states. Table 9 shows clearly that group 3 transition-metal oxide cations have O-atom affinities lower than those for the group 4 metal oxide cations, while those for the group 5 metal oxide cations are highest. The OAs for the other transition-metal oxide cations available in Table 9 are all quite high and larger than those for 3B transition-metal oxide cations. The reason is related to their electronic structures. The group 3 cations only have two electrons to bind the first oxygen and no capabilities left for the second, and group 4 cations have one electron left for the second, while other transition cations have at least two electrons left for the second.

The metal dioxide cations MO_2^+ did not appear to react further with D_2O to produce trioxide cations under our experimental operating conditions. The OD group affinities for the metal−oxide cations HfO^+ and ZrO^+ are not currently available, but our observation of OD transfer to these cations with D_2O suggests that they must be larger than $D(DO-D) = 121.2$ kcal mol^{-1}.

4. Conclusion

The experimental scan of the D_2O reactivity with 46 atomic cations from the fourth, fifth, and sixth rows of the periodic table has characterized the periodicities in the reactivities of these atomic cations at room temperature. O-Atom transfer occurs in the reactions of the early transition meal cations (Sc^+, Ti^+, La^+, Ti^+, Zr^+, Hf^+, V^+, Nb^+, Ta^+, Mo^+, and W^+) and one main-group cation (As^+); OD transfer occurs with only three cations (Sr^+, Ba^+, and La^+). Other cations, including most late transition cations and the main-group cations, mostly react by slow D_2O addition or not at all. Competitive reactions occur for only a few cations: OD transfer competes with O-atom transfer in the reaction with La^+, and D_2O addition competes with O-atom transfer in the reactions with V^+, Nb^+, Mo^+, and As^+ and with OD transfer in the reaction with Sr^+.

The efficiency for O-atom transfer is not predictable by thermodynamics alone. Exothermic O-atom transfer reactions with atomic cations in high-spin states often exhibit low reaction efficiencies, and these can be understood in terms of barriers introduced by the change in spin required to proceed from the reactant to the product potential energy surfaces.

Secondary and higher-order reactions lead to the further oxidation of Nb^+, Ta^+, Mo^+, and W^+ to form MO_2^+ and further OD group transfer with Zr^+ and Hf^+ to form MO_2D^+. Further D_2O addition occurs with $M^+(D_2O)$, MO^+, MOD^+, MO_2^+, and MO_2D^+ to form $M^+(D_2O)_n$ ($n \leq 5$), $MO^+(D_2O)_n$ ($n \leq 5$), $MOD^+(D_2O)$, $MO_2^+(D_2O)_n$ ($n \leq 5$), and $MO_2D^+(D_2O)_n$ ($n \leq 4$). Up to five D_2O molecules add sequentially to selected atomic M^+ and MO^+ as well as MO_2^+ and four to MO_2D^+. Equilibrium measurements for sequential D_2O addition to M^+ indicate that the periodic variation in reaction efficiency (k/k_c) parallels the periodic variation in the standard free binding energy ($\Delta G°$).

Acknowledgment. Continued financial support from the Natural Sciences and Engineering Research Council of Canada is greatly appreciated. Also, we acknowledge support from the National Research Council, the Natural Science and Engineering Research Council, and MDS SCIEX in the form of a Research Partnership grant. As holder of a Canada Research Chair in Physical Chemistry, D.K.B. thanks the contributions of the Canada Research Chair Program to this research.

References and Notes

(1) Koyanagi, G. K.; Caraiman, D.; Blagojevic, V.; Bohme, D. K. *J. Phys. Chem. A* **2002**, *106*, 4581.
(2) Caraiman, D.; Bohme, D. K. *J. Phys. Chem. A* **2002**, *106*, 9705.
(3) Caraiman, D.; Koyanagi, G. K.; Bohme, D. K. *J. Phys. Chem. A* **2004**, *108*, 978.
(4) Lavrov, V. V.; Blagojevic, V.; Koyanagi, G. K.; Orlova, G.; Bohme, D. K. *J. Phys. Chem. A* **2004**, *108*, 5610.
(5) Koyanagi, G. K.; Bohme, D. K. *J. Phys. Chem. A* **2006**, *110*, 1232.
(6) Cheng, P.; Koyanagi, G. K.; Bohme, D. K. *J. Phys. Chem. A* **2006**, *110*, 2718.
(7) Zhao, X.; Koyanagi, G. K.; Bohme, D. K. *J. Phys. Chem. A* **2006**, *110*, 10607.
(8) Johnsen, R.; Brown, H. L.; Biondi, M. A. *J. Chem. Phys.* **1971**, *55*, 186.
(9) Magnera, T. F.; David, D. E.; Michl, J. *J. Am. Chem. Soc.* **1989**, *111*, 4100.
(10) Chen, Y.-M.; Clemmer, D. E.; Armentrout, P. B. *J. Phys. Chem.* **1994**, *98*, 11490.
(11) Sanekata, M.; Misaizu, F.; Fuke, K.; Iwata, S.; Hashimoto, K. *J. Am. Chem. Soc.* **1995**, *117*, 747.
(12) MacTaylor, R. S.; Vann, W. D.; Castleman, A. W., Jr. *J. Phys. Chem.* **1996**, *100*, 5329.
(13) Mikhailov, V. A.; Barran, P. E.; Stace, A. J. *Phys. Chem. Chem. Phys.* **1999**, *1*, 3461.
(14) Koyanagi, G. K.; Bohme, D. K.; Kretzschmar, I.; Schröder, D.; Schwarz, H. *J. Phys. Chem. A* **2001**, *105*, 4259.
(15) Baranov, V.; Javahery, G.; Hopkinson, A. C.; Bohme, D. K. *J. Am. Chem. Soc.* **1995**, *117*, 12801.
(16) Guo, B. C.; Kerns, K. P.; Castleman, A. W., Jr. *J. Phys. Chem.* **1992**, *96*, 4879.
(17) Clemmer, D. E.; Chen, Y.-M.; Khan, F. A.; Armentrout, P. B. *J. Phys. Chem.* **1994**, *98*, 6522.
(18) Clemmer, D. E.; Chen, Y.-M.; Aristov, N.; Armentrout, P. B. *J. Phys. Chem.* **1994**, *98*, 7538.
(19) Chen, Y.-M.; Clemmer, D. E.; Armentrout, P. B. *J. Am. Chem. Soc.* **1994**, *116*, 7815.
(20) Dalleska, N. F.; Tjelta, B. L.; Armentrout, P. B. *J. Phys. Chem.* **1994**, *98*, 4191.
(21) Dalleska, N. F.; Honma, K.; Sunderlin, L. S.; Armentrout, P. B. *J. Am. Chem. Soc.* **1994**, *116*, 3519.
(22) Searles, S. K.; Kebarle, P. *Can. J. Chem.* **1969**, *47*, 2619.
(23) Dzidic, I.; Kebarle, P. *J. Phys. Chem.* **1970**, *74*, 1466.
(24) Kebarle, P. *J. Chem. Phys.* **1970**, *53*, 2129.
(25) Irigoras, A.; Elizalde, O.; Silanes, I.; Fowler, J. E.; Ugalde, J. M. *J. Am. Chem. Soc.* **2000**, *122*, 114.
(26) Irigoras, A.; Fowler, J. E.; Ugalde, J. M. *J. Am. Chem. Soc.* **1999**, *121*, 574.
(27) Irigoras, A.; Fowler, J. E.; Ugalde, J. M. *J. Am. Chem. Soc.* **1999**, *121*, 8549.
(28) Chiodo, S.; Kondakova, O.; Michelini, M. d. C.; Russo, N.; Sicilia, E.; Irigoras, A.; Ugalde, J. M. *J. Phys. Chem. A* **2004**, *108*, 1069.

(29) Musaev, D. G.; Xu, S.; Irle, S.; Lin, M. C. *J. Phys. Chem. A* **2006**, *110*, 4495.
(30) Irikura, K. K.; Beauchamp, J. L. *J. Phys. Chem.* **1991**, *95*, 8344.
(31) Koyanagi, G. K.; Lavrov, V. V.; Baranov, V.; Bandura, D.; Tanner, S.; McLaren, J. W.; Bohme, D. K. *Int. J. Mass Spectrom.* **2000**, *194*, 1.
(32) Raksit, A. B.; Bohme, D. K. *Int. J. Mass Spectrom. Ion Processes* **1983**, *55*, 69.
(33) Mackay, G. I.; Vlachos, G. D.; Bohme, D. K.; Schiff, H. I. *Int. J. Mass. Spectrom. Ion Phys.* **1980**, *36*, 259.
(34) Koyanagi, G. K.; Baranov, V. I.; Tanner, S. D.; Bohme, D. K. *J. Anal. At. Spectrom.* **2000**, *15*, 1207.
(35) Moore, C. E. *Atomic Energy Levels as Derived from the Analyses of Optical Spectra*; U.S. National Bureau of Standards (NSRDS-NBS 35): Washington, DC, 1971.
(36) Van Kleef, T. A. M.; Metsch, B. C. *Physica C* **1978**, *95*, 251.
(37) Condon, E. U.; Shortley, G. H. *The Theory of Atomic Spectra*; Cambridge University Press: Cambridge, 1963.
(38) Caraiman, D.; Koyanagi, G. K.; Cunje, A.; Hopkinson, A. C.; Bohme, D. K. *Organometallics* **2002**, *21*, 4293.
(39) Koyanagi, G. K.; Bohme, D. K. *Int. J. Mass Spectrom.* **2003**, *227*, 563.
(40) Calculation from the NIST database; http://webbook.nist.gov/chemistry.
(41) Su, T.; Chesnavich, W. J. *J. Chem. Phys.* **1982**, *76*, 5183.
(42) Maryott, A. A.; Buckley, F. *Natl. Bu. Stand. Circ. (U.S.)* **1953**, 29.
(43) Dyke, T. R.; Muenter, J. S. *J. Chem. Phys.* **1973**, *59*, 3125.
(44) Clemmer, D. E.; Aristov, N.; Armentrout, P. B. *J. Phys. Chem.* **1993**, *97*, 544.
(45) Marinelli, P. J.; Squires, R. R. *J. Am. Chem. Soc.* **1989**, *111*, 4101.
(46) Schultz, R. H.; Armentrout, P. B. *J. Phys. Chem.* **1993**, *97*, 596.
(47) Minas da Piedade, M. E.; Martinho Simoes, J. A. *J. Organomet. Chem.* **1996**, *518*, 167.
(48) Baranov, V.; Bohme, D. K. *Int. J. Mass Spectrom. Ion Processes* **1996**, *154*, 71.
(49) Fiedler, A.; Kretzschmar, I.; Schröder, D.; Schwarz, H. *J. Am. Chem. Soc.* **1996**, *118*, 9941.
(50) Schröder, D.; Schwarz, H.; Shaik, S. *Struct. Bonding (Berlin)* **2000**, *97*, 91.
(51) Lias, S. G.; Bartmess, J. E.; Liebman, J. F.; Holmes, J. L.; Levin, R. D.; Mallard, W. G. *J. Phys. Chem. Ref. Data* **1988**, *17*, 861.
(52) Freiser, B. S. *Organnometallic Ion Chemistry*; Kluwer: Dordrecht, The Netherlands, 1996.
(53) Sievers, M. R.; Chen, Y.-M.; Armentrout, P. B. *J. Chem. Phys.* **1996**, *105*, 6322.
(54) Chen, Y.-M.; Armentrout, P. B. *J. Chem. Phys.* **1995**, *103*, 618.
(55) Clemmer, D. E.; Dalleska, N. F.; Armentrout, P. B. *Chem. Phys. Lett.* **1992**, *190*, 259.
(56) Beyer, M. Stability and Reactivity of Oxo- and Peroxorhenium Cations: Investigation of Elementary Steps in Homogeneous Catalysis, Diploma Thesis, Physics Department, TU München, Garching, 1996.
(57) Irikura, K. K.; Beauchamp, J. L. *J. Am. Chem. Soc.* **1989**, *111*, 75.
(58) Pavlov, M.; Blomberg, M. R. A.; Siegbahn, P. E. M.; Wesendrup, R.; Heinemann, C.; Schwarz, H. *J. Phys. Chem. A* **1997**, *101*, 1567.
(59) Blagojevic, V.; Koyanagi, G. K.; Lavrov, V. V.; Orlova, G.; Bohme, D. K. *Chem. Phys. Lett.* **2004**, *389*, 303.
(60) Zhang, X.-G.; Armentrout, P. B. *J. Phys. Chem. A* **2003**, *107*, 8904.
(61) Armentrout, P. B. *Int. J. Mass Spectrom.* **2003**, *227*, 289.
(62) Pettersson, L. G. M.; Bauschlicher, C. W., Jr.; Langhoff, S. R.; Partridge, H. *J. Chem. Phys.* **1987**, *87*, 481.
(63) Ohanessian, G.; Brusich, M. J.; Goddard, W. A., III. *J. Am. Chem. Soc.* **1990**, *112*, 7179.
(64) Parke, L. G.; Hinton, C. S.; Armentrout, P. B. *Int. J. Mass Spectrom.* **2006**, *254*, 168.
(65) Armentrout, P. B.; Li, F.-X. *J. Chem. Phys.* **2004**, *121*, 248.
(66) Li, F.-X.; Zhang, X.-G.; Armentrout, P. B. *J. Phys. Chem. B* **2005**, *109*, 8350.
(67) Li, F.-X.; Armentrout, P. B. *J. Chem. Phys.* **2006**, *125*, 133114.
(68) Kochanski, E.; Constantin, E. *J. Chem. Phys.* **1987**, *87*, 1661.
(69) Rosi, M.; Bauschlicher, C. W., Jr. *J. Chem. Phys.* **1990**, *92*, 1876.
(70) Lee, H. M.; Tarakeshwar, P.; Park, J.; Kolaski, M. R.; Yoon, Y. J.; Yi, H.-B.; Kim, W. Y.; Kim, K. S. *J. Phys. Chem. A* **2004**, *108*, 2949.
(71) Kebarle, P. *Ann. Rev. Phys. Chem.* **1977**, *28*, 445.
(72) Koizumi, H.; Larson, M.; Muntean, F.; Armentrout, P. B. *Int. J. Mass Spectrom.* **2003**, *228*, 221.
(73) Poisson, L.; Lepetit, F.; Mestdagh, J. M.; Visticot, J. P. *J. Phys. Chem. A* **2002**, *106*, 5455.